Astron. Astrophys. 361, 283–292 (2000)

ASTRONOMY
AND
ASTROPHYSICS

The atmospheres of cool, helium-rich white dwarfs

U.G. Jørgensen[1], **D. Hammer**[2], **A. Borysow**[1,⋆], **and J. Falkesgaard**[1]

[1] Niels Bohr Institute, Astronomical Observatory, Juliane Maries vej 30, 2100 Copenhagen, Denmark
[2] Department of Physics, The University of Texas at Austin, Austin, TX 78712, USA

Received 10 May 2000 / Accepted 16 June 2000

Abstract. We have modified our version of the MARCS stellar atmosphere code to make it possible to compute white dwarf atmospheres, and we have constructed and present here the necessary input data for such calculations. With this new tool we have computed a number of helium-rich white dwarf atmospheres, synthetic spectra, and broad band colours, and we compare them here with observational data from the literature.

The major differences between our code and existing white dwarf codes in the literature, are (1) a detailed computation of the chemical equilibrium between all relevant ions, neutral atoms, and molecules, (2) a detailed line-by-line calculation of the molecular opacity, and (3) a detailed quantum mechanical description of the collision-induced absorption (CIA) processes.

The molecular line data include a few hundred million spectral lines from CO, CH, CN, CS, C_2, C_3, C_2H, HCN, and C_2H_2. The sampling of the lines is done by the opacity sampling (OS) method. The CIA data are calculated from *ab initio* dipole and potential surfaces suitable for high temperatures. Results for the H_2-H_2 absorption coefficient have been presented elsewhere, while the H_2-He CIA data are obtained specifically for this study, and are presented at frequencies from 800 to 20 000 cm^{-1} and at temperatures from 1 000 to 7 000 K. The new data are available at www.astro.ku.dk/∼aborysow/programs/.

Our code is particularly useful for description of the cooler white dwarfs. These have received increased attention during recent years because of better observational facilities. They are important for understanding the conditions in the early phase of the evolution of our Galaxy and as a tool to determine the age of the Galactic disk and halo. We demonstrate the importance of including all elements (i.e. not only hydrogen and helium as is done in several existing models in the literature), and of including collision-induced opacities and molecular line opacities in the atmospheric models. Our results are in good agreement with existing photometry of cool white dwarfs. In particular, we can explain the scatter in observational colour-colour diagrams as a consequence of small variations in the C/O ratio. Finally we discuss, based on our new models, the possible role of molecular C_2H in so-called C_2H white dwarfs.

Send offprint requests to: U.G. Jørgensen (uffegj@nbi.dk)

⋆ On professional leave of absence from Physics Department, Michigan Technological University, Houghton, MI, 49931, USA

Key words: stars: white dwarfs – molecular data – stars: atmospheres – infrared: stars

1. Introduction

When the remnant of the interior of a star enters the white dwarf cooling sequence, it is hot and bright. Historically, white dwarf research has therefore been focused on hot, high density material. With the increasing capacity of modern telescopes, dimmer and dimmer objects have been within observational reach. For white dwarfs, intrinsic low luminosity also means that they are cool and old. Today, the observational abilities are close to the possibility of observing the coolest possible white dwarfs, i.e. the remnants of the oldest stars that formed during the creation of the Galactic disk, or even during the formation of the halo. This has obviously caused a strong increase in the interest in the coolest white dwarfs (see e.g., Bergeron et al. 1994, Weidemann & Koester 1995, Ruiz 1996, Hansen 1998, Harris et al. 1999, Chabrier 1999).

With good model atmospheres describing these coolest white dwarfs it is possible to transform the observed colours or spectra of these stars into effective temperatures, and with good cooling tracks (e.g., D'Antona & Mazzitelli 1990, Hansen & Phinney 1998, Hansen 1999) it is possible to transform such effective temperatures into ages, and thus determine for example the age of our Galaxy or of the star-forming epoch of the Galactic disk.

Because the brightest white dwarfs were also the hottest, model atmospheres presented in the literature were developed to describe the atmosphere of hot objects. In this case, detailed description of atomic resonance lines and non-LTE effects are important for the model structure, and have to be treated with all possible accuracy. With the increasing interest in the cool white dwarfs, some of the existing model atmosphere codes have, during recent years, been modified in an attempt to include also some of the processes that are important in cool objects. However, these codes generally still lack a detailed description of the molecular opacities, which is very essential for cool stars.

For a number of years we have worked with a model atmosphere code, the MARCS code, which was from the start specifically developed for describing cool giant stars. This code has

the advantage over traditional white dwarf model atmosphere codes, that it has a very detailed description and handling of the molecular equilibrium and opacities. On the other hand, it for example does not account for non-LTE effects which play a role only for warmer stars. We have updated the code so that it is applicable also for the higher densities of white dwarf atmospheres, and in the present paper we describe results of applying this new version of the code to calculations of the atmospheres of cool white dwarfs.

Often cited cool white dwarf model atmospheres include those by Bergeron et al. (1995, 1997 - hereafter BRL97), Saumon & Jacobson (1999), Hansen (1999), and Bues & Aslan (1997, see also Aslan & Bues 2000). The models of Bergeron et al., of Hansen, and those of Saumon & Jacobson are computed for pure hydrogen, pure helium or mixed hydrogen and helium gases, and are very advanced and detailed in the description of these gases. Compared to these models a major advantage of our new white dwarf model atmospheres is the addition of all elements other than hydrogen and helium and the formation of all relevant molecules that can form out of these elements. The models of Bues & Aslan include H, He, C, N, and O, and molecules formed of these. The major advantage of our models compared to theirs is a more complete and detailed description of the molecular equilibrium and opacities, and the inclusion of CIA opacities due to H_2-H_2 and H_2-He (preliminary estimates of CIA are included in the models by Bergeron et al., by Hansen, and by Saumon & Jacobson, but not in the models of Bues & Aslan).

White dwarfs are carbon rich, and we have therefore applied our extensive molecular line list data base of carbon rich molecules, which was traditionally used to describe carbon stars. With a few exceptions, the molecules that dominate the line opacity in cool white dwarfs are the same as those that determine the structure in carbon star giants and dwarfs. The equilibrium between these molecules is however quite different in white dwarfs from that in the giants. We have therefore developed a new chemical equilibrium routine for the present study of white dwarfs.

For many cool white dwarfs the gas pressure is dominated by helium, and we have therefore, for the present work, developed a detailed quantum mechanical description of the H_2-He collision-induced transitions and the corresponding absorption coefficient. Details are given in Sect. 3. Advanced models for CIA due to H_2–He pairs at high temperatures have been unavailable until the present work. The extent to which earlier estimates for H_2–He CIA, involving numerous approximations (Borysow et al. 1997), give reliable results has until the present work been largely unknown. Although we concentrate in this paper on the helium-rich cool white dwarfs, we compute, for comparison, also a few hydrogen-rich ones, and the most up-to-date H_2–H_2 CIA (Borysow et al. 2000) have been included in all our models.

The presented models are the first white dwarf models in the literature which include full molecular equilibrium, collision-induced absorption processes, and detailed line-by-line treatment of all relevant molecular opacities.

2. The model atmosphere computation

The model atmospheric structures were computed by use of an updated version of the MARCS stellar atmospheric code, which iteratively solves the model atmosphere problem in a radiative and convective scheme. The original version of the code has been described by Gustafsson et al. (1975), and most of the improvements of relevance for the present study, which are not described in the present paper, have been described by Jørgensen et al. (1992) and Jørgensen (1997). The chemical equilibrium routine we usually apply for computations of the main sequence and giant stars with the MARCS code, was found to be highly insufficient for the modelling of cool white dwarfs, and we have consequently developed a new routine based on totally new fits to the latest version of the JANAF thermo-chemical data (the latest version is unpublished, while the latest published version can be found in Chase et al. 1985). The new routine computes the chemical equilibrium between all relevant neutral atoms, several ions, and more than 200 molecules. It will be described in detail in Falkesgaard & Jørgensen (2000, in preparation). Results based on the new routine differ substantially from the old ones for high gravities and for very cool objects, but for giant stars the new results are almost identical to results based on the old routine.

By choosing this approach together with our extensive molecular line list data base developed for studies of carbon stars, we have been able to compute models that take full account of all relevant molecules formed in white dwarfs, except for the C_2H molecule (which will be described in detail in Sect. 7) for which an appropriate line list still doesn't exist.

The line list data are sampled with the use of the opacity sampling (OS) technique. For the synthetic spectra and broad band colour calculations we use an OS resolution of 20 000, whereas we usually have adopted a factor of approximately 10 lower resolution for the model computation (resulting in approximately 10 000 adopted OS frequency points throughout the spectrum for the model calculations). This is the first time that a detailed treatment of molecular lines has been included in white dwarf model atmosphere computations. The more sparse amount of molecular opacity data which is included in the models of Bues & Aslan is based on the JOLA smearing out average method. For giant stars average methods in the treatment of the opacity data have been shown to lead to substantial errors in the model structure (see for example Jørgensen 1992 where also the JOLA method and comparisons with the opacity sampling method have been described in detail). No similar tests exist for white dwarf atmospheric models, where one can expect the differences between the results of the two sampling methods to be somewhat smaller than for giants, due to the higher densities of the white dwarf atmospheres.

The adopted abundances in our test computations were close to those inferred from observations of cool He-rich white dwarfs by several authors (Zeidler-K.T. 1987, Weidemann & Koester 1995, Schmidt et al. 1995, Koester & Allard 1996, Bues & Aslan 1997), i.e. $N(He)/N(H) \approx 10^5$, $N(O)/N(He) \approx 10^{-6}$, $C/O > 1$, and the ratios of the number of all other elements over

helium down by a factor of approximately 10^6 compared to the corresponding solar ratios.

3. CIA *ab initio* calculations

3.1. Introduction

CIA is a significant supermolecular absorption process whenever high densities ($\gtrsim 10^{20}$ molecules per cm^3) are considered. It is particularly striking in environments composed of neutral, infrared inactive molecules (for an overview see Frommhold 1993). CIA is caused by time-varying, collision-induced supermolecular dipole moments. Thus the calculation of CIA spectra requires as input the induced dipole surface and a good model of the interaction potential of the colliding pair of atoms or molecules. For the simpler systems, such as H_2–He, advanced quantum chemical methods permit very accurate calculations of these surfaces which may then be used to determine the collision-induced spectral intensities and profiles (Frommhold 1993, Meyer & Frommhold 1995). If high temperatures are considered, these theoretical surfaces must be known accurately for many collisional separations and angular orientations of the molecules with respect to the inter-collisional axis, and for many vibrational spacings of the interacting molecules. Thus thousands of lengthy quantum chemical calculations must be run so that at present only one complete high-temperature study exists, investigating collision-induced *emission* in the H_2–He system (Hammer et al. 1999). Using the same *ab initio* dipole and potential surfaces we determine here collision-induced *absorption* spectra at temperatures from 1 000 to 7 000 K. Although those high-temperature *ab initio* calculations could not be of the same precision as some of the earlier studies optimised for cool environments (Meyer & Frommhold 1995, Frommhold 1993) because of the added complexity, the reliability of the spectra presented here exceeds greatly that of the only known early, semi-empirical (Patch 1971,1974) or quantum mechanical (Borysow & Frommhold 1989, Borysow et al. 1989, 1988) investigations of CIA of H_2-He at high temperatures.

3.2. Ab initio dipole surface and potential

We use the previously obtained Cartesian components of the induced dipole moment $\mu_{x,y,z}(r, R, \vartheta)$ and the interaction potential surface $V(r, R, \vartheta)$ for various separations and orientations of the collisional H_2–He system; r and R designate intramolecular and intermolecular separations, respectively, and ϑ is the angle subtended by the inter- and intramolecular axes. Analytic fits are derived from the $\mu_{x,y,z}$ for the spherical dipole tensor components $A_{\lambda L}(r, R)$ of symmetry λ,L, according to

$$\mu_\nu(\mathbf{r}, \mathbf{R}) = \frac{4\pi}{\sqrt{3}} \sum_{\lambda,L} A_{\lambda L}(r, R) \sum_{m_\lambda, m_L} C(\lambda L 1; m_\lambda m_L \nu) \times Y_{\lambda m_\lambda}(\widehat{r})\, Y_{1\nu}(\widehat{R})\,. \quad (1)$$

The spherical dipole components μ_ν are related to the Cartesian ones by $\mu_0 = \mu_z$ and $\mu_{\pm 1} = \mp(\mu_x \pm i\mu_y)/\sqrt{2}$. The $Y_{\ell m}(\vartheta, \varphi)$ are the spherical harmonics; the $C(j_1 j_2 j_3; m_1 m_2 m_3)$ are Clebsch-Gordan coefficients; $\widehat{r}$ is a unit vector in the direction of the intramolecular axis $\mathbf{r}$; $\widehat{R}$ is a unit vector in the direction of the intercollisional axis $\mathbf{R}$. Using the five lowest order terms of the summation over λ and L, λ,L = 0,1; 2,1; 2,3; 4,3; 4,5 was found to be sufficient for a good representation of the spectra. Similar to the dipole moment, the interaction potential is expanded into a sum over spherical harmonics, yet only the isotropic term $V_{00}(r, R)$ is retained. Further details are discussed by Hammer et al. (1999).

For the computation of the collision-induced spectra, matrix elements of the potential (V) and dipole (A) surfaces are needed for rotovibrational transitions $|vJ\rangle \rightarrow |v'J'\rangle$ (v is the vibrational and J the rotational quantum number of the H_2 molecule; a prime indicates final states),

$$B_{\lambda L}^{vJv'J'}(R) = \langle vJ\,|A_{\lambda L}(r, R)|\,v'J'\rangle \quad (2)$$

$$V_{00}^{vv}(R) = \langle v0\,|V_{00}(r, R)|\,v0\rangle\,. \quad (3)$$

Here, $|vJ\rangle$ represents only the radial part of the rotovibrational wave-functions of H_2; angular integrations are performed analytically. From previous work (Borysow et al. 1990) we know that the centrifugal distortion of the vibrational wave-functions cannot be ignored for our calculations. Thus the radial rotovibrational wave-functions of H_2 for $v = 0, 1, 2, \ldots, 7$ and a number of rotational states are obtained as needed from the intra-molecular H_2 potential of Kolos et al. (1986) using a Numerov algorithm; the necessary integrations, Eqs. (2), (3), are performed numerically.

3.3. Spectra

The collision-induced absorption coefficient (in cm^{-1}) as function of angular frequency ω is given by Frommhold (1993)

$$\alpha(\omega) = \frac{4\pi^2}{3\hbar c}\, \varrho_1\, \varrho_2\, N_L^2\, \omega\, (1 - \exp(-\hbar\omega/kT))\, g_a(\omega; T)\,; \quad (4)$$

ϱ_1 and ϱ_2 are the densities of the hydrogen and helium gas in amagat; $N_L = 2.68 \times 10^{19}$ cm^{-3} is Loschmidt's number which corresponds to a number density of one amagat; and $g_a(\omega; T)$ is the spectral density function,

$$g_a(\omega; T) = \sum_{\lambda,L} \sum_{v,J,v',J'} P_{vJ}(T) \times G_a(\omega - \omega_{v',J,v',J'}; T, v, J, v', J')\,; \quad (5)$$

$\omega_{v'J'vJ} = (E_{v'J'} - E_{vJ})/\hbar$ is the transition frequency of the transition $|vJ\rangle \rightarrow |v'J'\rangle$ and $P_{vJ}(T)$ is the population probability of the initial rotovibrational state,

$$P_{vJ}(T) = Z(T)^{-1}\, (2J + 1)\, g_J\, \exp(-E_{vJ}/kT)\,, \quad (6)$$

where $Z(T) = \sum_{vJ}(2J + 1)\, g_J\, \exp(-E_{vJ}/kT)$ is the partition function and g_J are the statistical weights due to nuclear spin: $g_J = 1$ for even J and $g_J = 3$ for odd J. The function $g_a(\omega)$ consists of a number of superimposed rotovibrational, diffuse lines $G_a(\bar{\omega})$ arising from transitions $|vJ\rangle \rightarrow |v'J'\rangle$ where $v,\ v'$ = 0, 1, 2,. . .,7. The shape of those lines for each transition could have been obtained from an existing quantum line shape

code (Frommhold 1993) using the $B_{\lambda L}^{vJv'J'}(R)$ and $V_{00}^{vv}(R)$ determined above, Eqs. (2, 3). However, since we had to include hundreds of different transitions and since the individual spectral line profiles do not depend much on the exact v, J, v', J' values – only the line intensities do – we chose a more economical approach: The integrated line intensities for each dipole matrix element $B_{\lambda L}^{vJv'J'}$ of symmetry λ,L can readily be obtained with high accuracy (especially at elevated temperatures) from a classical sum formula (see Frommhold 1993),

$$M_{\lambda L}^{vJv'J'} = 4\pi \int_0^\infty \exp(-V_{00}^{vv}(R)/kT) \times \left[B_{\lambda L}^{vJv'J'}(R)\right]^2 R^2\, dR\,, \qquad (7)$$

so that only a few line profiles for transitions $v \rightarrow v'$, with $J = J' = 0$ had to be computed. Using those quantum line shapes and integrated intensities, the latter for all transitions to be included, we computed the absorption spectra, Eq. (4), as superposition of the (normalised) line shapes $G_a(\bar{\omega})$, which were centred at the appropriate rotovibrational transition frequencies, Eq. (5), and multiplied by the respective zeroth moments, Eq. (7), and the population probability of the initial rotovibrational state, Eq. (6). Further details may be found in Frommhold (1993) and in Hammer et al. (1999).

3.4. Comparison with an earlier high temperature CIA model

In Fig. 1 we compare our new quantum mechanical data with earlier high-temperature H_2–He CIA spectra (Borysow et al. 1997), which were obtained from models by Borysow et al. (1988, 1989) and Borysow & Frommhold (1989) by applying semi-empirical corrections to those models.

The apparent big differences between the new computations and those of Borysow et al. (1997), of up to a factor of ten or more, require some comments. Whereas both, the new and the old results, are based on quantum mechanical computations, the details of the approaches differ. In the previous computations an old collision-induced dipole surface (Frommhold & Meyer 1987) and isotropic interaction potential (Schäfer & Köhler 1985) were used, which allowed for the computations of the necessary vibrational matrix elements, Eqs. (2,3), but were suitable for low temperature spectra only. The J-dependence of the spectra was not taken into account, since at that time the importance of that was not obvious. In order to represent the numerical functions $G_a(\bar{\omega})$, model line shapes were used, which satisfied certain symmetry conditions required for CIA spectra. However, it is well known that the reliability of such line shapes is limited, and is "guaranteed" only within an intensity range of approximately 100:1; their behaviour in the far wings is unpredictable and causes the huge discrepancies between the spectra observed at 7 000 K. The differences between the two sets of data at frequencies beyond 15 000 cm^{-1} are enhanced by the complete neglect of $\Delta v = 4$ transitions in the earlier computations. The original models existed at temperatures up to 7 000 K, except for the rototranslational band, for which they extended only up to 3 000 K (Borysow et al. 1988) so that in this case

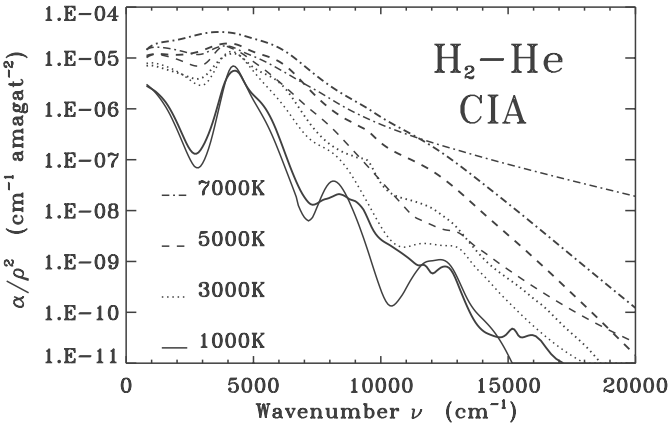

Fig. 1. Comparison of old (thin lines) and new (thick lines) H_2–He CIA spectra.

extrapolation to higher temperatures was necessary. Finally, the previous calculations had to be corrected for the missing contributions of transitions with $v > 0$, which become increasingly important at high temperatures. This was accomplished by a simple rescaling of the spectra with a temperature-dependent population factor (Borysow et al. 1997), which was, of course, a somewhat uncertain *ad hoc* solution.

However, the new calculations still contain some inaccuracies. For the high temperatures considered in this work and in Hammer et al. (1999), dipole and potential surface of the H_2–He system had to be determined for a large number of inter- and intra-molecular distances. So, for economical reasons the accuracy of earlier, low-temperature calculations (Frommhold 1993) could not be achieved. The dipole surface used here is believed to be accurate within about 10%, rendering the spectra (which depend on the square of the dipole) accurate to about 20% — at maximum intensity. With increasing frequency the uncertainty is expected to increase. The inaccuracy of the *ab initio* data is likely to be responsible for the "wiggles" in the 1 000 K spectrum around 12 000 cm^{-1} and 15 000 cm^{-1}, but they are still within the numerical noise level.

To summarise, we see differences between the spectra from previous and present calculations of up to a factor of ten (and in some cases even more), which are understandable considering the numerous approximations involved in the earlier approach. Those differences are bigger than the uncertainties of the current, more precise calculations. However, the lower the temperatures and the lower the frequencies, the better the agreement between the two results.

4. The model atmospheric structure

Fig. 2 shows (as solid line) the temperature versus gas pressure structure for a model atmosphere of $T_{\rm eff}$ = 3000 K, $\log g$ = 8, C/O = 1.02, ϵ_{He} = 17.5 (i.e., the number density of helium equal $10^{17.5}$ on a scale where the number density of hydrogen is 10^{12}), and the ratio of most other elements compared to helium down by a factor 10^6 compared to the corresponding solar ratios. Also shown are the atmospheric structures when

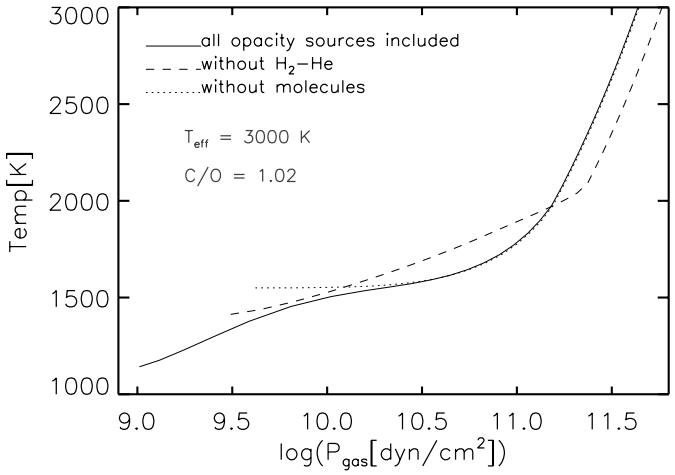

Fig. 2. Model atmospheric structures of a helium-rich white dwarf with $T_{\rm eff}$ = 3000 K, $\log g$ = 8, C/O = 1.02, ϵ_{He} = 17.5, and ϵ_O = 11.5. Dashed line represents a model where the H_2-He CIA opacity has been excluded from the model computation, while solid line represents a model with all opacity sources included. Dotted line represents a model where the molecules have been excluded from the opacity.

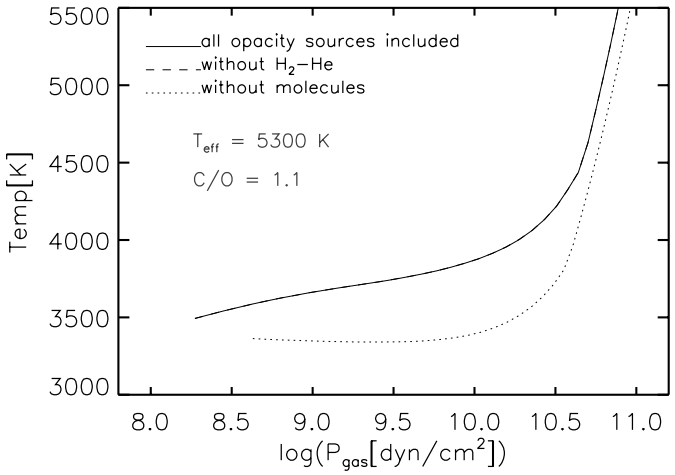

Fig. 3. Same as Fig. 2, but for models with $T_{\rm eff}$ = 5300 K (the dashed and the solid lines are identical to within the accuracy of the plot).

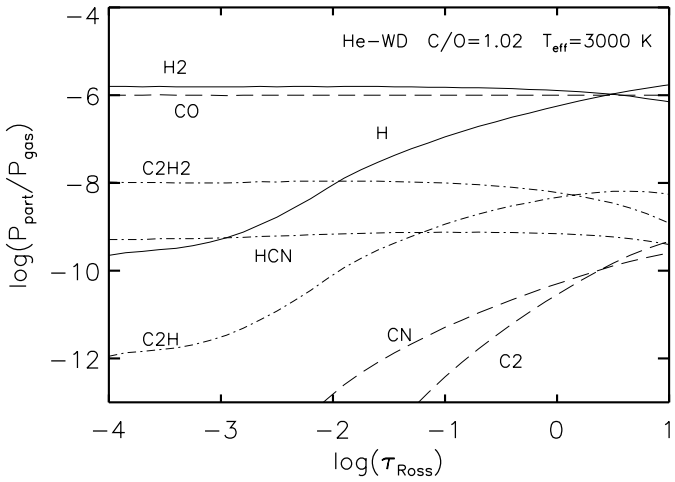

Fig. 4. The partial pressures of various molecules for the full opacity model atmosphere shown in Fig. 2. The partial pressures of H and H_2 are shown as solid lines, diatomics (except H_2) are shown as dashed lines, while polyatomics are shown by dash-dot lines. The names of the molecules are marked along the curves.

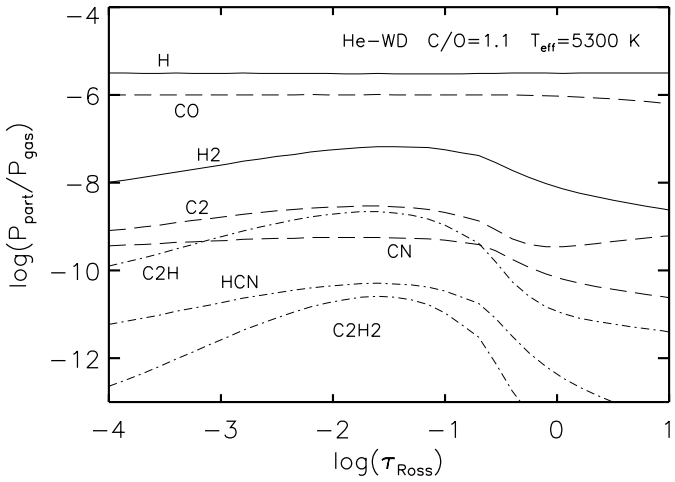

Fig. 5. The partial pressures of various molecules (and neutral hydrogen) as in Fig. 4, but here for the model atmosphere in Fig. 3.

the H_2−He CIA opacity is excluded (dashed line) and when all molecular opacities (except the CIA opacities) are excluded (dotted line). The lower left end of the curves represent the top of the atmosphere, where both the temperature and gas pressure are lowest. In all models, the Rosseland mean optical depth is approximately $10^{-4} - 10^{-5}$ there.

It is seen from Fig. 2 that the effect of including molecular opacities in the model computation is a substantial expansion and cooling of the upper part of the atmosphere. Also CIA causes an expansion and cooling of the upper part of the model. In addition, CIA creates a cooling of the layers a bit deeper (around log(P_g) = 10 − 11 in this case) where the CIA opacity due to the high density is substantial. A corresponding heating of the interior of the model, which ensures a flux constancy, is also seen in the figure. The flux distributions corresponding to the two models in Fig. 2 with (solid lines) and without (dashed lines) H_2−He CIA in the atmospheres and the spectrum computations, will be presented in Fig. 6.

In Fig. 3 we show the corresponding effects as in Fig. 2, but now for a model with $T_{\rm eff}$ = 5300 K and C/O = 1.1. It is seen that at this effective temperature the CIA no longer plays a role for the model structure. The molecules are still important contributers to the opacity, but at these higher temperatures it is no longer the polyatomic molecules that influence the structure, but rather diatomic molecules such as CO, CN, C_2 and CH. For this reason the effect of the molecules is no longer a cooling of the atmosphere, as was the case for the $T_{\rm eff}$ = 3000 K model, but on the contrary a substantial heating, as is seen in Fig. 3.

In Figs. 4 and 5 we show some of the partial pressures corresponding to the model in Fig. 2 (i.e., $T_{\rm eff}$ = 3000 K, $\log g$ = 8.0, C/O = 1.02, and N(He)/N(H) = $10^{5.5}$) and Fig. 3 (i.e., $T_{\rm eff}$

= 5300 K, $\log g$ = 8.0, C/O = 1.1, and N(He)/N(H) = $10^{5.5}$). H and H_2 are shown as solid lines, while diatomic molecules are indicated by dashed lines, and polyatomics by dash-dotted lines. The partial pressures are shown normalised to the total gas pressure, which (since N(He)/N(H) = $10^{5.5}$) is almost identical to the partial pressure of He.

It is seen that in the $T_{\rm eff}$ = 3000 K model the abundance of H_2 dominates over H with up to 4 orders of magnitude. Therefore H_2-He CIA becomes a dominant opacity source in this model. In contrast, the ratio P(H_2)/P(H) $\lesssim 10^{-2}$ in the $T_{\rm eff}$ = 5300 K, and therefore neither H_2-H_2 nor H_2-He CIA will be a strong opacity source in this model.

It is also recognised from Figs. 4 and 5 how the ratio between polyatomic molecules and diatomic molecules decrease drastically when the effective temperature of the model is increased from 3000 K to 5300 K, which explains the different response the two models have to the inclusion of molecules (respectively, a temperature decrease and a temperature increase in the upper part of the atmosphere). However, still in the $T_{\rm eff}$ = 5300 K model the partial pressures of several molecules are relatively high. For example, the partial pressure of C_2 is only approximately one order of magnitude smaller than that of H_2 throughout most of the atmosphere. Since the integrated absorption coefficient of C_2 per molecule is several orders of magnitude stronger than that of H_2-H_2 or H_2-He CIA per pair of absorbers, the opacity of C_2 strongly dominates over the CIA opacities at such effective temperatures.

If carbon and other "metals" were left out as an opacity source, the model structure would adjust itself until the model found a new equilibrium structure with another source taking up the necessary absorption. In a zero-metallicity model this absorption would often be CIA because it involves only hydrogen and helium, which have very little other absorption possibilities under such conditions. For this reason the role of CIA in our white dwarf atmospheres is restricted to somewhat lower effective temperatures than has previously been found in the literature, based on models of pure hydrogen and/or helium compositions (e.g., Bergeron et al. 1995, 1997, Saumon & Jacobson 1999, Lenzuni et al. 1991).

As a consequence of the non-zero-metallicity, our models also include a detailed treatment of all electron donors, which give rise to a much higher number density of electrons than in models based on pure hydrogen and/or helium. Potassium and sodium (K and Na) are the main electron donors in most regions of the $T_{\rm eff}$ = 3000 K model presented above, while both Fe, Mg, Na, and Al contribute to the $T_{\rm eff}$ = 5300 K model. In the warmest layers near the bottom of both models, also ionised carbon contributes to the electron density. In no region of any of the models do hydrogen and helium contribute with more than 5% of the total number of free electrons, and in the bulk of the atmospheres the combined contribution by H and He to the number of electrons, is considerably below 0.1 percent. The number of free electrons significantly affects the abundance of He^- and H^- which are the dominant continuum absorbers in our models, and since furthermore scattering on free electrons is the dominant continuum scattering process, our models are of course sensitive to the metallicity, and are very different from corresponding zero-metallicity models in the literature.

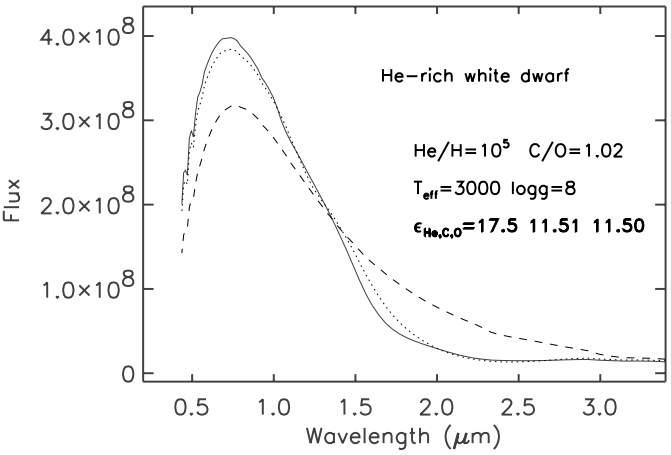

Fig. 6. The flux distribution (in erg/cm^2/s/μm) for He-rich models with $T_{\rm eff}$ = 3000 K and C/O = 1.02, computed based on (1) our new H_2-He opacities (solid line), (2) the old H_2-He estimate (dotted line) and (3) without H_2-He in the opacity at all (dashed line).

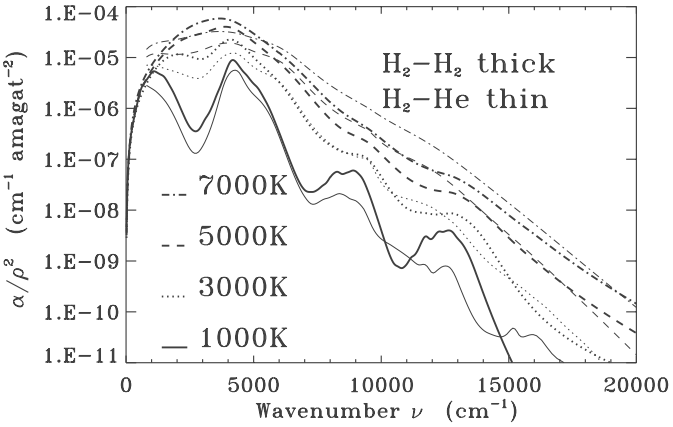

Fig. 7. Comparison of the most recent H_2-H_2 and H_2-He CIA absorption coefficients.

5. The synthetic spectra

In Fig. 6 we show the computed flux distribution of the models from Fig. 2 computed with (solid line) and without (dashed line) the H_2-He CIA opacity. Also shown are the results of the corresponding computation based on our older estimate of the H_2-He absorption coefficient (which has been used in several earlier white dwarf models, e.g. BRL97). It is seen that the major difference between the results based on the new and the old H_2-He absorption coefficient is in the 1.5−2.0 μm region (the H band filter region) and around the flux maximum (here in the R band region).

In Fig. 7 we compare our new H_2-He data with the corresponding new H_2-H_2 data from Borysow et al. (2000). We see that the H_2-He and H_2-H_2 absorption coefficients are surprisingly similar to one another (in particular in the important temperature region around 3000 K), in contrast to our older and

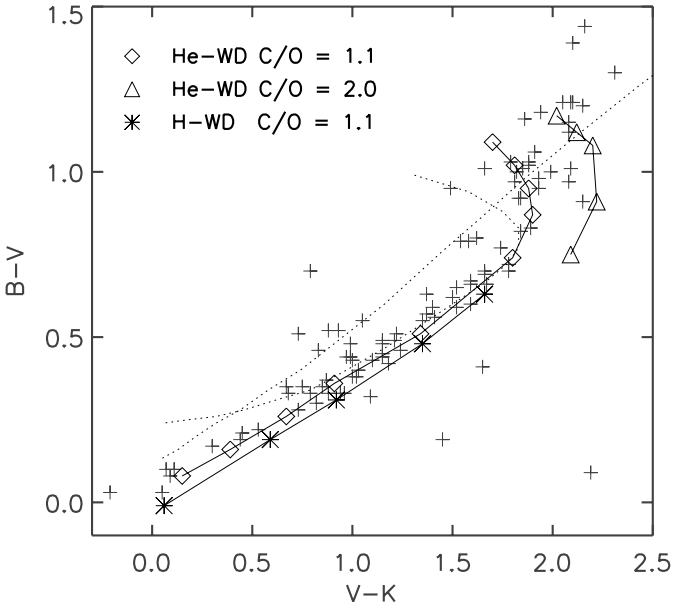

Fig. 8. The B-V versus V-K colour-colour diagram for our computed helium-rich white dwarf models (solid lines), compared to the pure helium and pure hydrogen models of BRL97 (dotted lines) and observed colours of white dwarfs (crosses). The different symbols of our models correspond to C/O = 1.1 (diamonds) and C/O = 2.0 (triangles). For comparison, are also shown our hydrogen-rich models (asterisks).

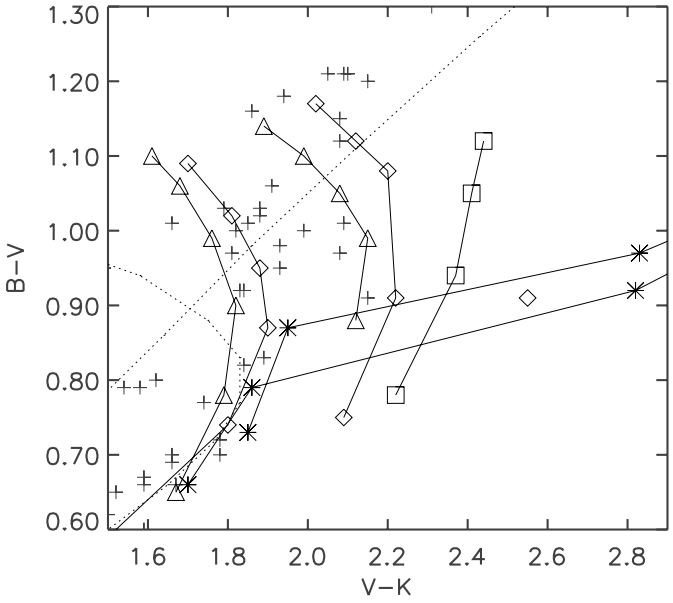

Fig. 9. Detail of Fig. 8, but showing additional models. From left to right the sequences of symbols connected by solid lines are models for C/O = 1.02 (triangles), 1.1 (diamonds), 1.6 (triangles), 2.0 (diamonds), 3.0 (squares) and 10.0 (a single diamond to the right in the diagram). Also shown in this figure is the effect (on the C/O = 1.02 and 1.1 models) of excluding H_2-He CIA from the opacity (asterisks).

more preliminary CIA data. This means that for cooler models of a given metallicity where CIA dominates the opacity, the spectra and colours will be almost independent of the the H/He ratio.

6. The broad band colors

In Figs. 8 and 9 we show the computed V−K versus B−V colour-colour diagram for our new models (various symbols connected by solid lines), compared to observations (crosses) and the pure hydrogen and the pure helium models of BRL97 (Bergeron et al. 1997) (dotted lines). Our models in Fig. 8 marked with diamonds are for C/O = 1.1 and range from $T_{\rm eff}$ = 9000 K in the lower left corner, over 8000 K, 7000 K, 6300 K, 5300 K, 4300 K, 3800 K, 3300 K, 3000 K, to 2800 K for the uppermost model in the sequence. The corresponding models for C/O = 2.0 (triangles) are for $T_{\rm eff}$ = 4300 K, 3800 K, 3300 K, and 2800 K. The hydrogen-rich models (asterisks) have N(H)/N(He) = 10^3, $Z/Z_\odot = 10^{-5}$, except for carbon which is increased so that C/O = 1.1. These models are for $T_{\rm eff}$ = 10 000 K, 8000 K, 7000 K, 6000 K, and 5000 K, from lower left toward upper right in the diagram. The almost straight dotted line are the pure helium models, while the curved dotted line is for pure hydrogen models (of BRL97).

Comparing our helium and hydrogen-rich models with the pure helium and pure hydrogen models of BRL97 we see several things: In the warm end of the sequences, we notice that both our hydrogen and our helium-rich models follow better the tendency of a linear sequence that the observations indicate, than do the warmer pure hydrogen BRL97 models which diverge toward higher values of B−V than observations for low V−K. We also notice that our helium-rich sequence falls more along the bulk of the observations than do the corresponding pure helium BRL97 models in the warmer (left) region of the diagram.

However, the main difference between the BRL97 models and our model sequence is for the cooler models (the upper right part of the diagram). The BRL97 pure helium models fall along an almost straight line in this colour-colour diagram, while the observations scatter in the diagram much more than the observational uncertainty. Introducing the full detailed and self-consistent description of the metallicity that our models have, allows to vary several parameters (the individual abundances of all elements) as possible explanations of the observational scatter. In particular, the carbon to oxygen ratio is likely to vary from star to star because of details in the mixing processes in the stars (e.g. MacDonald et al. 1998). When full molecular equilibrium and opacities are included in the models, the colours are very sensitive to the exact C/O ratio, because of the large dissociation energy of the CO molecule which causes most of the carbon (when C/O > 1) to be locked up in CO. We therefore computed series of models with different carbon abundances (but all other abundances fixed), such that C/O varied between 1.02 and 10.0.

Fig. 8 illustrates the effect of the varying C/O ratio for models with C/O = 1.1 and C/O = 2.0. In Fig. 9 we focus on the cool region of V−K > 1.5, and illustrate the effect for a few more C/O ratios. The sequences from left to right in this figure correspond to C/O = 1.02 (triangles ∼ models of $T_{\rm eff}$ = 4300 K, 3800 K, 3300 K, 3000 K, 2800 K, 2700 K from the lower to the upper end of the plotted sequence), C/O = 1.1 (diamonds ∼ $T_{\rm eff}$ =

4300 K, 3800 K, 3300 K, 3000 K, 2800 K), C/O = 1.6 (triangles $\sim T_{\rm eff}$ = 3800 K, 3500 K, 3300 K, 3000 K, 2800 K), C/O = 2.0 (diamonds $\sim T_{\rm eff}$ = 4300 K, 3800 K, 3300 K, 3000 K, 2800 K), C/O = 3.0 (squares $\sim T_{\rm eff}$ = 4300 K, 3800 K, 3300 K, 3000 K), and C/O = 10 (a single diamond $\sim T_{\rm eff}$ = 4300 K). We see that a modest variation in C/O (from 1.02 to 2.0) together with a realistic scatter in effective temperature (between $\approx$ 3000 K and 4000 K) can explain the scatter in the cool end of the diagram. The stars with the higher C/O ratios are positioned toward the right in the diagram, and the coolest ones are positioned toward the top of the diagram.

We notice from Fig. 7 that our new H_2-He CIA is very similar to the detailed H_2-H_2 CIA of Borysow et al. (2000). As mentioned above this causes the cool models where CIA dominates to be quite insensitive to the H/He ratio, in contrast to models in the literature based on our more preliminary estimates of the collision induced absorption coefficients. Our warmer models are also relatively insensitive to the H/He ratio, as is seen in Fig. 8. This is because in our models the electron density comes mainly from the metals, and only very few electrons come from hydrogen and helium. In zero-metallicity models, on the other hand, the electrons obviously have to come from either hydrogen or helium, and the different ionization potential of these two atoms are then responsible for a quite different electron density and corresponding different structure of models dominated by hydrogen and models dominated by helium. In the regime where our models are dominated by molecular line absorption, the structure, spectrum and colours can be sensitive to the H/He ratio, but only if the hydrogen abundance is extremely low. In that case the abundance of hydrocarbon molecules depends on the available hydrogen rather than on the available excess carbon after the CO formation. When the H/He ratio decreases, the abundance of molecules such as CH, C_2H_2, C_2H will decrease relative to molecules such as C_2, C_3, CN, and other non-hydrogen containing molecules. In this way the H/He ratio obviously can play an important role for the opacity. The BRL97 sequence most to the right in Fig. 8 and Fig. 9 represents their pure helium models. These do not show any CIA (because there is no hydrogen, and thus no H_2). Due to the pronounced lack of opacity, these models become very compact in their structure, and the absorption is mainly due to processes which are not relevant in our models where the processes described above dominate the opacity even for very small amounts of hydrogen and metals.

In the warm end of the sequences shown in Fig. 8 we attribute the differences between our models and those of BRL97 to our more detailed description of the metallicities which, as described above, has an important effect on the electron densities and the continuum absorption and scattering. In the cooler end of the sequences the major difference between our models and the BRL97 models is due to our inclusion of a detailed description of the molecular formation and opacities, which gives rise to a large change in the colours when the abundances of different contributing molecular species vary, in particular as function of the C/O ratio. Also our inclusion of a more accurate absorption coefficient of H_2-H_2 and H_2-He CIA, as described above, contributes to the differences, in particular for the very coolest objects.

Compared to the models of Aslan & Bues (2000) we estimate C/O ratios considerably closer to unity than what their models predict. A major difference between their models and ours is our inclusion of collision-induced absorption, which is neglected in the Aslan & Bues models. In Fig. 9 we show the effects on the BVK colours of excluding CIA from the opacity in our models and spectra (asterisks). The lowest and most left of these models is for C/O = 1.02 and $T_{\rm eff}$ = 4300 K. The two other models with larger values of V−K and B−V in the sequence are for $T_{\rm eff}$ = 3800 K and $T_{\rm eff}$ = 3300 K (and C/O = 1.02). The corresponding models with $T_{\rm eff} < 3300$ K are out of the diagram. It is seen that the effect of CIA on the $T_{\rm eff}$ = 4300 K model is marginal, giving rise to an increase in V−K as well as in B−V of only approximately 0.02 mag. (although the effect is of course larger for colours where the absorption of CIA is larger, as can be understood for example from Fig. 6). For the $T_{\rm eff}$ = 3800 K model the effect is larger, and is seen from Fig. 9 to amount to approximately 0.1 mag. in V−K. For the 3300 K model the difference between the model with and without CIA is a full magnitude in V−K, with the model without CIA being completely out of the region of observed stars in the diagram. Similar numbers are seen to hold for the C/O = 1.1 sequence of models, which also range from $T_{\rm eff}$ = 4300 K over 3800 K to 3300 K from the left to the right in the figure.

7. The question of C_2H in "C_2H white dwarfs"

A small class of DQ cool white dwarfs are usually termed "C_2H white dwarfs" in the literature, based on the existence of three characteristic absorption features around 5000 Å. These bands have actually not really been identified as being due to C_2H, because neither laboratory measurements nor theoretical computations exist identifying bands of C_2H in this spectral region. The suggestion of the bands being due to C_2H is based on a chemical equilibrium computation by Schmidt et al. (1995) which shows C_2H to be abundant in pure H/He/C gases of temperatures around 5000 to 6000 K and gas pressures around $P_g = 10^9$ dyn/cm^2. We present here a more complete molecular equilibrium computation, which includes molecules from all relevant elements and which treats the model atmosphere and spectrum computations self-consistently.

We have shown in Fig. 4 and 5 that for cool white dwarfs of C/O close to 1 the abundance of C_2H is 2 to 4 orders of magnitude smaller than that of C_2H_2 and HCN (for the parameters in Fig. 4), and that for warmer models with C/O $\approx$ 1.1 (Fig. 5) the partial pressure of C_2H is comparable or somewhat smaller than that of C_2. It is obvious that there is a tendency for C_2H to become relatively more important for decreasing $T_{\rm eff}$ and for increasing C/O, which is also what we should expect, because decreasing $T_{\rm eff}$ favours polyatomics over diatomics and increasing C/O favours molecules with more than one carbon atom. In Fig. 10 we therefore plot the partial pressures for our extreme model with C/O = 10 (and $T_{\rm eff}$ = 4300 K). It is seen that in this model the partial pressure of C_2H does dominate over

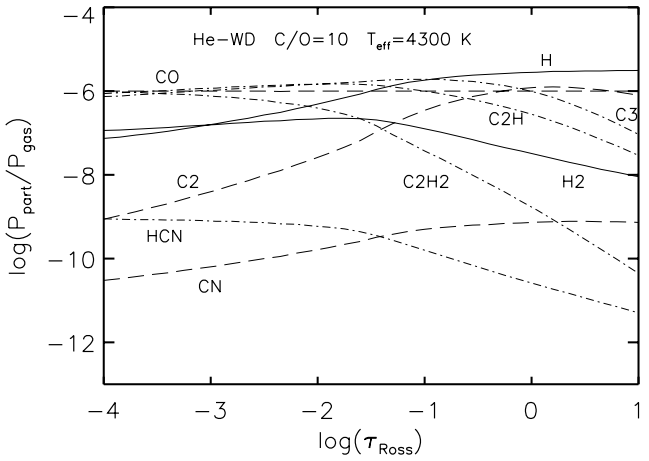

Fig. 10. The partial pressures of various molecules marked along the curves, for a helium-rich model with $T_{\rm eff}$ = 4300 K and C/O = 10.

those of HCN and C_2H_2 in most of the atmosphere, although the molecule C_3 has an even higher partial pressure at such high values of C/O.

A general problem with the interpretation of the possible existence of C_2H in stellar spectra is lacking experimental data, and confusion in the theoretical interpretation of the C_2H spectrum. The geometry of the molecule is not clear, and it has not been possible to even assign quantum numbers to several of the few lines that have been observed in the laboratory. One of the complications is that the first excited electronic state is lower than several of the vibrational eigen-energies of the electronic ground state, and that this unusual overlap between the values of vibrational and electronic energies is strongly dependent on the excitation of the vibrational bending mode (due to an unusually large anharmonicy; see for example Reimers et al. 1985). A summary of the problems and the present theoretical and observational status has recently been given by Peyerimhoff (1994).

Goebel et al. (1983) computed a low resolution (R $\approx$ 60) absorption coefficient of the A←X electronic transition in C_2H, based on the CASSCF *ab initio* theory, and predicted the two strongest bands at 2500 K to be at $\lambda \approx 2.7\mu$m and $\approx 1.5\mu$m. This calculation indicates that the integrated infrared absorption coefficient of C_2H is approximately a factor of 10 larger than that of C_2H_2 (or HCN or C_3). This is, however, still more than a factor of 10 smaller than the integrated absorption coefficient of C_2. The main reason that the absorption coefficient of C_2H is so much stronger than the corresponding C_2H_2/HCN/C_3 absorption coefficients, is that it is an electronic transition, as opposed to the others, which are pure vibrational transitions. Also the relevant C_2 systems are electronic transitions.

The predicted 1.5μm band may have been seen in the spectra of carbon-rich giant stars (Lancon & Wood 2000), and the 2.7μm band may have been seen in the carbon-rich giant star HD 19557 (Goebel et al. 1983). Our own computations with an OS absorption coefficient of the C_2H band at 2.7μm (based on the work of Goebel et al.) included in the synthetic spectrum calculations show slightly better agreement with the observed ISO spectra of the carbon-rich giant star TX Psc than the results we have presented recently (Jørgensen et al. 2000) without this band. Our C_2H OS absorption coefficient is (in contrast to all the other molecules included) not based directly on a line list, since such one does not exist, as mentioned above. Instead, several different scalings have been used.

However encouraging these results of possible identifications in stars might seem, Reimers et al. (1985) (overlapping with the authors in the paper of Goebel et al. 1983) recalculated the absorption coefficient, and found quite different results for the position of the bands in the C_2H electronic system. A central new aspect in this calculation was the realization that the combination of large thermal bending amplitude and high bending frequency of the $^2A'$ component of the A state gives rise to a substantial blue shift which increases with temperature. Hence, at 3000 K the peak of the predicted A←X absorption coefficient was now at 1.1 μm instead of the 2.7 μm in the old calculations, with the bulk of the absorption in the region from 0.8 μm to 1.5 μm. In addition, Reimers et al. computed also the pure vibrational transitions, which they found to be much weaker than the A←X band, and situated in the 2.5−3.0 μm region and at longer wavelengths. No authors have yet predicted absorption from C_2H in the 5000 Å region (but admittedly none have claimed that such an absorption system could not be possible either; only very little is known).

Our own calculations presented in Figs. 4, 5, and 10 show that if C_2H is to have considerably stronger bands than those of C_2 (which have the strong Swan-system close to the position of the proposed 5000 Å C_2H bands) and stronger than the other polyatomic carbon molecules in the infrared (which have bands in the same region as the C_2H A←X system), the "C_2H white dwarfs" have to be both very cold and with very high C/O ratios. However, the observations seem to indicate effective temperatures in the range of 5000 K to 7000 K (Schmidt et al. 1995) which, although still cold in terms of white dwarfs, are too warm to show pronounced C_2H abundances according to our calculations. Furthermore, the high C/O $\approx$ 10 necessary in order to have abundant C_2H as shown in Fig. 10, is in contradiction with the photometry of existing white dwarfs according to our model predictions shown in Fig. 9. Although all these results do not strictly exclude that C_2H can be responsible for the bands seen in "C_2H white dwarfs", they do not make it likely.

Aslan & Bues (2000) speculated that absorption from quasi-molecular He_2 may be the source of the 5000 Å bands in "C_2H white dwarfs", but as for C_2H a major problem is again that the value of the absorption coefficient of He_2 is unknown in the visual region. In addition, the partial pressure of He_2 cannot be computed from chemical equilibrium because the molecule has no stable ground-state, and in the work of Aslan & Bues (2000) the abundance of He_2 is therefore instead inferred from a scaling to the abundance of C_2.

8. Conclusions

We have computed new model atmospheres for cool helium-rich (and a few hydrogen-rich) white dwarfs. Our models differ from most other cool white dwarf models in the literature by a

detailed computation of the chemical equilibrium between all relevant ions, neutral atoms, and molecules, together with a detailed line-by-line description of the molecular opacity and a detailed quantum mechanical calculation of the collision-induced absorption processes.

As a consequence of the inclusion of all elements, we find that the electron density is determined by the ionization of Fe, Mg, K, Na, Al, and C. Less than 0.1% of the electrons come from hydrogen and helium, and our models are therefore relatively insensitive to the H/He ratio, unless when the abundance of hydrogen is comparable to or smaller than the abundance of carbon minus oxygen in which case the H/He ratio influences the relative molecular abundances. The similarity between the hydrogen and the helium dominated models is also more pronounced than in older white dwarf models because our new H_2-H_2 and H_2-He absorption coefficients are more similar to one another than previous calculations indicated. While the new H_2-H_2 absorption coefficient was published elsewhere, new calculations of the H_2-He absorption coefficient were presented here. New high-temperature dipole and potential surfaces for the H_2–He system have allowed a considerably more reliable calculation of the CIA spectra for this system than those previously known, and the new data differ from older values for the H_2-He system by a factor of 10 or more at important frequencies and temperatures.

Our resulting white dwarf models are in good agreement with observations of cool white dwarfs from the literature. We presented a complete $B-V$ versus $V-K$ diagram of all cool white dwarfs in the literature, and demonstrated that the bulk of the stars can be explained by a sequence of our models with effective temperatures between 9000 K and 2800 K. As opposed to zero-metallicity models, our models can explain the observed scatter in the colour-colour diagrams. In particular the observed scatter in the presented BVK colours can be reproduced by models with a variation in the C/O ratio between 1.02 and 2.0.

Finally, we commented on the results of a self-consistent calculation concerning the effects of the molecule C_2H, and concluded that the likelihood of C_2H being responsible for pronounced spectral features usually attributed to C_2H in so-called C_2H white dwarfs, is very small. The existing data for this molecule are, however, much poorer than the data for other molecules of importance for cool white dwarfs, due to an extraordinarily complicated chemical structure of this molecule, and better laboratory data as well as *ab initio* data for C_2H are urgently needed in order to improve the situation.

Acknowledgements. We acknowledge the support from NASA, Astrophysics Theory Program (grant # NAG5-3689), the Danish Natural Science Research Council, and, for the work in Texas, the R. A. Welch Foundation, grant # 1346. We thank L.Frommhold for valuable discussions concerning the collision-induced absorption calculations, and S.Langhoff for discussions concerning the C_2H absorption coefficient.

References

Aslan T., Bues I., 2000, A&A, preprint
Bergeron P., Ruiz M.-T., Leggett S.K., Saumon D., Wesemael F., 1994, ApJ 423, 456
Bergeron P., Saumon D., Wesemael F., 1995, ApJ 443, 764
Bergeron P., Ruiz M.-T., Leggett S.K., 1997, ApJS 108, 339
Borysow A., Frommhold L., 1989, ApJ 341, 549
Borysow J., Frommhold L., Birnbaum G., 1988, ApJ 326, 509
Borysow A., Frommhold L., Moraldi M., 1989, ApJ 336, 495
Borysow A., Frommhold L., Meyer W., 1990, Phys. Review A 41, 264
Borysow A., Jørgensen U.G., Zheng C., 1997, A&A 324, 185
Borysow A., Jørgensen U.G., Fu Y., 2000, J. Quant. Spectrosc. Radiat. Transfer, in press
Bues I., Aslan T., 1997, Ap&SS 251, 181
Chabrier G., 1999, ApJ 513, L103
Chase M.W., Davies C.A., Downey J.R., et al., 1985, J. Phys. Chem. Ref. Data 14, 1
D'Antona F., Mazzitelli I., 1990, ARA&A 28, 139
Frommhold L., 1993, Collision-induced Absorption in Gases. Cambridge University Press, Cambridge, New York
Frommhold L., Meyer W., 1987, Phys. Rev. A 35, 632
Goebel J.H., Bregman J.D., Cooper D.M., et al., 1983, ApJ 270, 190
Gustafsson B., Bell R.A., Eriksson K., Nordlund Å., 1975, A&A 42, 407
Hammer D., Frommhold L., Meyer W., 1999, J. Chem. Phys. 111, 6283
Hansen B.M.S., 1998, Nat 394, 860
Hansen B.M.S., 1999, ApJ 520, 680
Hansen B.M.S., Phinney E.S., 1998, MNRAS 294, 557
Harris H.C., Dahn C.C., Vrba F.J., et al., 1999, ApJ 524, 1000
Jørgensen U.G., 1992, Rev. Mex. Astron. Astrofis. 23,, 195
Jørgensen U.G., 1997, In: van Dishoeck E.F. (ed.) Molecules in Astrophysics: Probes and Processes. Kluwer, p. 441
Jørgensen U.G., Hron J., Loidl R., 2000, A&A 356, 253
Jørgensen U.G., Johnson H.R., Nordlund Å., 1992, A&A 261, 263
Koester D., Allard N.F., 1996, In: Jeffery C.S., Heber U. (eds.) Hydrogen-Deficient Stars. ASP Conf.Ser. vol. 96, p. 324
Kolos W., Szalewicz K., Monkhorst H.J., 1986, J. Chem. Phys. 84, 3278
Lancon A., Wood P., 2000, A&A, in press
Lenzuni P., Chernoff D.F., Salpeter E.E., 1991, ApJS 76, 759
Meyer W., Frommhold L., 1995, In: Tabisz G.C., Neuman M.N. (eds.) Collision- and Interaction-Induced Spectroscopy. Kluwer, Dordrecht, p. 441
MacDonald J., Hernanz M., José J., 1998, MNRAS 296, 523
Patch R.W., 1971, J. Quant. Spectrosc. Rad. Transfer 11, 1311
Patch R.W., 1974, J. Quant. Spectrosc. Rad. Transfer 14, 49
Peyerimhoff S.D., 1994, In: Jørgensen U.G. (ed.) Molecules in the Stellar Environment. LNP vol. 428, Springer, p. 326
Reimers J.R., Wilson K.R., Heller E.J., Langhoff S.R., 1985, J. Chem. Phys. 82, 5064
Ruiz M.-T., 1996, AJ 111, 1267
Saumon D., Jacobson S.B., 1999, ApJ 511, L107
Schmidt G.D., Bergeron P., Fegley B., 1995, ApJ 443, 274
Schäfer J., Köhler W.E., 1985, Physica 129 A, 469
Weidemann V., Koester D., 1995, A&A 297, 216
Zeidler-K.T.E.-M., 1987, A&AS 68, 469